20th Australasian Fluid Mechanics Conference
Perth, Australia
5-8 December 2016

# Large-Amplitude Flapping of an Inverted-Flag in a Uniform Steady Flow – a Vortex-Induced Vibration

**J. E. Sader[1], J. Cossé[2], D. Kim[3], B. Fan[2] and M. Gharib[2]**

[1]School of Mathematics and Statistics, The University of Melbourne, Victoria 3010, Australia
[2]Division of Engineering and Applied Science, California Institute of Technology, Pasadena, CA 91125, USA
[3]Department of Mechanical Engineering, KAIST, Daejeon, 305-701, South Korea

## Abstract

The dynamics of a cantilevered elastic sheet, with a uniform steady flow impinging on its clamped-end, have been studied widely and provide insight into the stability of flags and biological phenomena. Recent measurements by Kim *et al.* J. Fluid Mech. **736**, R1 (2013) show that reversing the sheet's orientation, with the flow impinging on its free-edge, dramatically alters its dynamics. In contrast to the conventional flag, which exhibits (small-amplitude) flutter above a critical flow speed, the inverted-flag displays large-amplitude flapping over a finite band of flow speeds. In this talk, we use a combination of mathematical theory, scaling analysis and measurement to establish that this large-amplitude flapping motion is a vortex-induced vibration. Onset of flapping is shown mathematically to be due to divergence instability, verifying previous speculation based on a two-point measurement. Reducing the sheet's aspect ratio (height/length) increases the critical flow speed for divergence and ultimately eliminates flapping. The flapping motion is associated with a separated flow – detailed measurements and scaling analysis show that it exhibits the required features of a vortex-induced vibration. Flapping is found to be periodic predominantly, with a transition to chaos as flow speed increases. Cessation of flapping occurs at higher speeds – increasing damping reduces the flow speed range where flapping is observed, as required. These findings have implications to leaf motion and other biological processes, such as the dynamics of individual hairs, because they also can present an inverted-flag configuration.

## Introduction

The stability of a cantilevered thin elastic sheet immersed in a steady uniform flow has received widespread attention due to its relevance in many applications, ranging from the aerodynamics of flight to understanding the basic dynamics of flag motion. The predominant configuration studied to date is that where the flow (i) impinges on the sheet's clamped end, and (ii) is parallel to the sheet; mimicking the orientation often encountered by flags and biological structures that naturally position themselves in the flow direction. This configuration will henceforth be referred to as the "conventional-flag" problem; as opposed to the "inverted-flag" reported by [6] which is the focus of this study. Shelley and Zhang [14] review the extensive body of literature on the conventional-flag problem. While this problem has been studied widely over the past century, the effects of orientation on the resulting sheet dynamics have received comparatively little attention.

Recent measurements by Kim *et al.* [6] show that reversing the orientation of a cantilevered thin elastic sheet, as per Fig. 1, with its length parallel to a steady uniform flow at high Reynolds numbers ($\mathrm{Re} \equiv UL/\nu \approx 10^4 - 10^5$), can dramatically alter the sheet's stability and resulting dynamics; $U$ is the flow speed, $L$ the sheet length, and $\nu$ the fluid's kinematic viscosity. The physical mechanisms underlying the observed behaviour of this

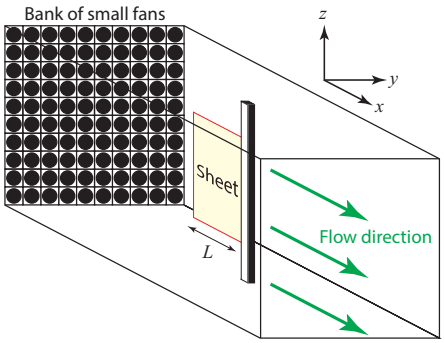


Figure 1: Schematic illustration of the measurement apparatus used to investigate the stability and dynamics of an inverted-flag in a uniform steady air flow. Sheet length, $L$, is shown and its height, $H$, is perpendicular to the flow (not shown).

inverted-flag remain unknown. The aim of this study is to shed light on these mechanisms and thus provide insight into the effects of flow orientation on a cantilevered elastic sheet's dynamics. We are not so much interested in modelling the complete flow, which in principle can be done using fully numerical or semi-analytical approaches developed previously, but using the most fundamental theoretical and experimental tools to extract the essential physics of the inverted-flag phenomenon. Indeed, while recent computational studies [5, 15, 11] were able to reproduce the phenomena observed experimentally, the dominant physical mechanisms were not described.

### Measurements as a function of the sheet's aspect ratio

Figure 2 presents stroboscopic measurements of the inverted-flag's motion, as a function of sheet height (and thus aspect ratio) and air flow speed; the dimensionless flow speed $\kappa$ is described below and defined in Eq. (1). These provide a direct extension of the measurements reported previously [6]. As described by Kim *et al.* [6], increasing the flow speed causes the sheet to move from a stable undeformed equilibrium to large-amplitude flapping. This occurs abruptly at a critical flow speed, $U_{\mathrm{lower}}$. When the flow speed is increased further, a second abrupt transition occurs at $U_{\mathrm{upper}}$ where large-amplitude flapping ceases and a steady deflection is recovered, at large-amplitude; a small amount of flutter is also observed in this deflected equilibrium.

These measurements, at constant sheet length, show that the sheet dynamics are strongly affected by the sheet's height, and thus its aspect ratio, with $U_{\mathrm{lower}}$ increasing with decreasing aspect ratio. In contrast, $U_{\mathrm{upper}}$ appears to be insensitive to the sheet's aspect ratio. This establishes that the sheet geometry can dramatically affect its dynamics, with flapping appearing only if the sheet's aspect ratio exceeds a critical value. For smaller aspect ratios, a direct transition to a stable deflected equilibrium occurs.

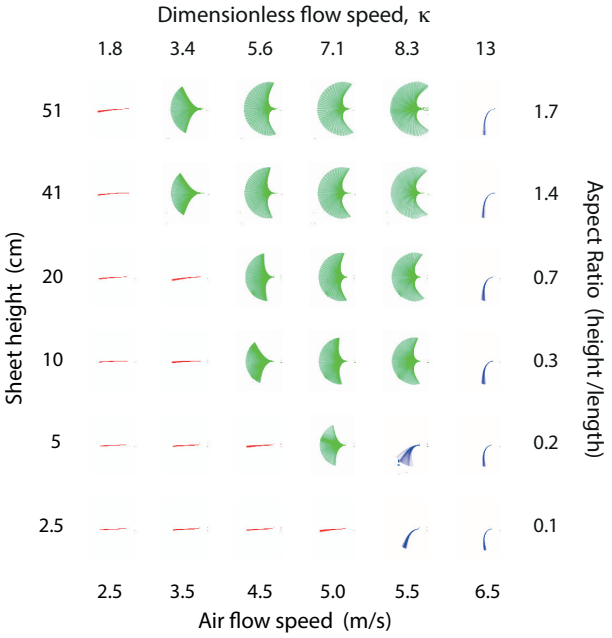


Figure 2: Stroboscopic images of the sheet motion as a function of sheet height and air flow speed, for sheet of length $L = 30$ cm. Dimensionless flow speed, $\kappa$, and sheet aspect ratio, $H/L$, are also indicated. Stable equilibrium states are observed at low (red) and high (blue) flow speeds, whereas large-amplitude flapping occurs at intermediate flow speeds (green). Flow direction is left-to-right, and the sheet is clamped at its right-hand end.

These results differ from those of a conventional-flag, which is always unstable above a critical flow speed [9, 14]. But the measurements in Fig. 2 are consistent with the findings of Rinaldi and Paidoussis [10], who considered the inverted-rod problem, i.e., a slender (cylindrical cross-section) elastic rod of small aspect ratio, which also did not display flapping behaviour. We now examine the physical mechanisms underlying the behaviour observed in Fig. 2.

### Stability at low flow speed

To begin, we investigate the onset of flapping at low flow speed, i.e., at $U_{\text{lower}}$. To theoretically explore the physical mechanisms driving $U_{\text{lower}}$, we draw on the study of Kornecki *et al.* [8]. As noted in Ref. [12], Argentina and Mahadevan [2] presented an analysis similar to that of Kornecki *et al.* [8], though this similarity has not been discussed in the literature previously.

To explore the sheet's stability at low flow speed, we initially study the limiting case of infinite aspect ratio, $H/L$; where $H$ and $L$ are the sheet height and length, respectively; see Fig. 1. This two-dimensional problem is relevant to understanding the practical case where the sheet's height greatly exceeds its length; see Fig. 1.

Kornecki *et al.* [8] and others (see Ref. [14] for a review) have shown that the stability of a conventional-flag depends on two parameters:

$$\kappa \equiv \frac{\rho U^2 L^3}{D}, \quad \mu \equiv \frac{\rho L}{\rho_s h}, \tag{1}$$

where $\kappa$ specifies the ratio of hydrodynamic to elastic restoring forces (henceforth referred to as the "dimensionless flow speed", for simplicity), and $\mu$ is the relative importance of fluid-to-solid inertia (termed the "added mass parameter"); $\rho$ is the fluid density, $\rho_s$ is the sheet density, $U$ is the flow speed, $h$ is the sheet thickness, and the sheet flexural rigidity is $D \equiv Eh^3/(12[1-\nu^2])$ where $E$ and $\nu$ are the Young's modulus and Poisson's ratio of the sheet.

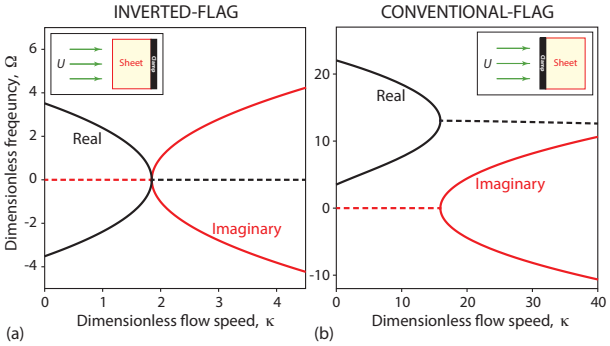


Figure 3: Stability of the zero-deflection equilibrium, for (a) an inverted-flag and (b) a conventional-flag. Dimensionless frequency, $\Omega$ [Eq. (2)] vs dimensionless flow speed, $\kappa$ are shown. A nonzero imaginary component indicates an unstable equilibrium.

While Ref. [8] used both steady and unsteady thin airfoil theory to account for the hydrodynamic load, we utilise the steady theory only here. This allows us to determine when steady and unsteady hydrodynamic processes are involved, while not unduly complicating the analysis [12]. Note that (unsteady) inertia in the solid sheet is included fully in both formulations.

The steady theory of Ref. [8] yields the following integrodifferential equation:

$$\frac{d^4 w}{dx^4} - \Omega^2 w + 2\kappa \frac{f(\theta) - f(0)}{\sin\theta} = 0, \tag{2}$$

where $w$ is the sheet deflection, $x$ the normalised Cartesian coordinate in the free-stream direction (scaled by the sheet length $L$), and the dimensionless frequency is defined

$$\Omega \equiv \omega \sqrt{\frac{\rho_s h L^4}{D}}, \tag{3}$$

where $\omega$ is the angular frequency of the sheet's motion, and

$$f(\theta) = \frac{1}{\pi} \int_0^\pi w'(\zeta) \frac{\sin^2\phi}{\cos\phi - \cos\theta} d\phi, \tag{4}$$

where $x = (1/2)(1+\cos\theta)$, $\zeta = (1/2)(1+\cos\phi)$, with $x \in [0,1]$ and $\theta, \phi \in [0, \pi]$; all other parameters are defined above.

Figure 3 shows the calculated (complex) frequencies, $\Omega$, for both the conventional- and inverted-flag problems, as a function of the dimensionless flow speed, $\kappa$. Emergence of a nonzero imaginary component defines the onset of an instability (bifurcation). While results for the conventional- and inverted-flags exhibit some obvious similarities, the striking difference is that the conventional-flag problem [Fig. 3(b)] bifurcates at nonzero frequency (see real part, at $\kappa = 15.9$), whereas stability of the inverted-flag [Fig. 3(a)] is lost at zero frequency when $\kappa = 1.85$. This analysis shows that, as the flow speed increases, the inverted-flag of infinite aspect ratio becomes unstable at $\kappa = 1.85$ due to the steady hydrodynamic lift-force balancing the elastic restoring force of the sheet – higher speeds cause it to deflect from its zero-deflection equilibrium position. The inverted-flag therefore exhibits a *divergence instability* [9]. The effect of this deflection on the sheet's subsequent dynamics is explored below.

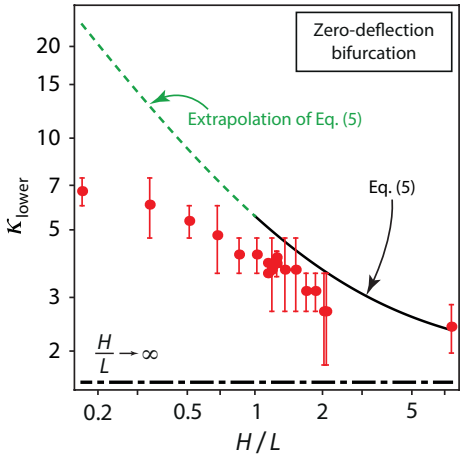


Figure 4: Bifurcation point of the zero-deflection equilibrium of an inverted-flag, showing the critical dimensionless flow speed, $\kappa_{lower}$, as a function of aspect ratio, $H/L$. Comparison of measurements in air [red dots] using sheets of length 5.1 and 30 cm, with the large aspect ratio ($H/L \geq 1$) formula Eq. (5) [solid black line]. The asymptotic limit $H/L \to \infty$ is indicated [dashed-dotted black line]. The (extrapolated) prediction of Eq. (5) is also shown for $H/L < 1$ [dashed black line]; this lies outside its range of validity and is given for reference only.

Because the bifurcation point of the zero deflection equilibrium is due to a steady fluid process, we can calculate the effect of finite aspect ratio, $H/L$, using Prandtl's lifting line theory,

$$\kappa_{lower} \equiv \rho U_{lower}^2 L^3/D \approx 1.85\left(1+\frac{2L}{H}\right), \qquad (5)$$

which is expected to hold for large aspect ratios, $H/L$ [12]. This equation predicts that the critical wind speed, $U_{lower}$, where the zero deflection equilibrium loses stability, increases as the sheet height decreases (at fixed length) – as observed in measurements; see Fig. 2.

Comparison of Eq. (5) to measurements is given in Fig. 4. Good agreement is found for large aspect ratios $H/L > 1$, with no adjustable parameters. This shows that the presented inviscid theory accurately captures the instability in these cases. However, Eq. (5) overestimates the measured value of $\kappa_{lower}$ for small aspect ratio, $H/L < 1$, where there appears to be an inflection in curvature. It is known that the sides of a wing generate vortices that can become trapped by the airflow and increase lift; the so-called 'vortex-lift' phenomenon [1]. Because this occurs at the sides, its effect on the overall lift will increase with decreasing aspect ratio, consistent with the discrepancy in Fig. 4.

### Flapping region

We turn our attention to the flapping phenomenon observed for $\kappa > \kappa_{lower}$. At these wind speeds, the zero deflection equilibrium is linearly unstable and the sheet spontaneously deflects. As the angle-of-attack of the sheet increases, the small-amplitude lifting flow [in Eq. (2)] separates [13]. Such flows are highly unsteady for the Reynolds numbers studied and exhibit periodic vortex shedding [13, 7, 16, 4]. Flow visualisation shows that sheet flapping is accompanied by synchronisation of periodic vortex shedding at the deflection maxima [6]. Such a fluid-structure interaction has been observed previously in the vortex-induced vibration of elastic cylinders [16, 4], which occurs by synchronisation of the vortex shedding frequency with the natural resonant frequency of the cylinder (in fluid).

Figure 5A gives the frequency at which the sheet oscillates in the flapping band, i.e., for $\kappa > \kappa_{lower}$. This shows that the frequency varies slightly but is significantly lower than the natural resonant frequency of the sheet with no flow. Such reduced frequency is expected because the fluid loading is strong ($\mu \approx 0.38$) and the impinging flow exerts a position dependent inertial load on the moving sheet under large-amplitude flapping. The maximum flapping frequency, $f_{res} \approx 8$ Hz, at $\kappa \approx 6$ coincides with the sheet exhibiting a maximum deflection oriented 90° to the wind direction. We note that constancy in the frequency of a vortex-induced vibration is only expected for light fluid loading, i.e., $\mu \ll 1$ [16, 4]. Both sheets violate this requirement – variation of the flapping frequency with wind speed is expected and observed.

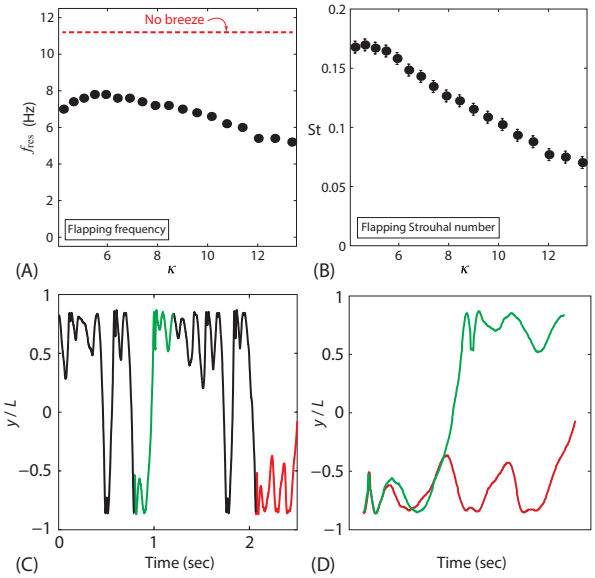


Figure 5: Flapping band dynamics for sheet: $L = 5.1$ cm & $H = 6.4$ cm. (A) Dominant flapping frequency, $f_{res}$, i.e., frequency with largest amplitude. (B) Associated Strouhal number. Error bars are smaller than symbols in A. (C) Time series of $y$-coordinate of sheet free end for $\kappa = 13.36$. (D) Green and red time segments in C are overlaid.

The Strouhal number is defined, $St \equiv f_{res}A/U$. Here, $A$ is the maximum vertical amplitude of flapping (peak-to-peak) to account for the deformable geometry of the flapping sheet and allow for comparison to previous studies on cylinders. Importantly, the Strouhal number, St, is related to $\kappa$: $A/L \approx 2St\sqrt{\kappa}\sqrt{1+1/\mu}$; effective mass enhancement of the sheet due to the fluid is approximated by the factor: $1+\mu$. An upper bound for $A/L$ is given by geometry. Periodic vortex shedding is required for a vortex-induced vibration, but occurs only above a critical sheet deflection. Assuming the value for a flat rigid sheet [7] applies here, gives the lower bound: $A/L|_{min} \approx 1/3$. We then obtain the required $\kappa$-region within which a vortex-induced vibration (VIV) can emerge:

$$\frac{\mu}{1+\mu} < \kappa < \frac{100\mu}{1+\mu}. \qquad (6)$$

Values of $\kappa$ outside this range require amplitudes that are either not possible geometrically (above the upper limit of this inequality), or do not allow the inverted-flag to exhibit periodic vortex shedding (below the lower limit).

The added mass parameter for the inverted-flags studied in Fig. 2 (in air) is $\mu = 0.38$, and thus Eq. (6) becomes

$$0.3 < \kappa < 30. \qquad (7)$$

Comparing this inequality with Eq. (5) (and the data in Fig. 4) shows that $\kappa_{\text{lower}}$ lies within the required flow speed range where a VIV can exist. This finding also holds true for inverted-flags immersed in water, corresponding to $\mu \gg 1$. We therefore conclude that a VIV can indeed be launched at $\kappa_{\text{lower}}$, for the measurements presented.

Figure 5B gives the Strouhal numbers in the flapping band. These are quantitatively similar to those reported previously [6] for a sheet six times longer in length, with very different vortex shedding frequencies. The Reynolds numbers in Ref. [6] are correspondingly six times larger, and thus the measurements in Fig. 5B probe a different flow regime. Strikingly, flapping begins at a Strouhal number of approximately 0.15 and decreases with increasing $\kappa$ until flapping ceases – such behaviour and values are typical for vortex-induced vibrations [7, 16, 4]. This similitude, the weak dependence of Strouhal number on Reynolds number, the weak variation in flapping frequency, the supression of flapping with enhanced damping (not shown here) [12], and the fact that $\kappa_{\text{lower}}$ lies within the range specified by Eq. (6), provide strong evidence that motion in the flapping band is a vortex-induced vibration [16, 4].

Sinusoidal motion is observed in the flapping band for low wind speeds $4.25 < \kappa < 11.4$. For higher values, $11.4 < \kappa < 13.4$, aperiodic motion emerges and intensifies with increasing wind speed – a sensitive dependence on initial conditions exists at the highest wind speed; see Fig. 5C-D. This establishes that the flag undergoes *chaotic dynamics* immediately prior to the abrupt emergence of a stable large-amplitude equilibrium at high wind speed; indicative of a nonlinear dynamical system, which is required for vortex-induced vibrations [16, 4]. The properties of the inverted-flag's chaotic motion, and its relation to chaos observed for a conventional-flag [3], presents an interesting area for further investigation.

## Conclusions

We have examined the physical mechanisms underlying the experimentally observed dynamics of an inverted-flag flapping in a uniform steady flow [6]. This was performed using a combination of theory, scaling analysis and experimental measurement; flow around the inverted-flag occurs in the high Reynolds regime ($\text{Re} \approx 10^4 - 10^5$).

Theoretical analysis of the zero-deflection equilibrium's stability shows that it exhibits a divergence bifurcation at low flow speeds. Measurements show that a reduction in the inverted-flag's aspect ratio (height/length) increases the critical flow speed where its zero-deflection equilibrium loses stability – a feature that is accurately predicted by the theory which is derived for aspect ratios greater than one. A strong deviation between the extrapolated predictions of this theory and measurement is observed for smaller aspect ratios, which is consistent with the presence of a vortex-lift phenomenon.

Measurements and analysis of the flapping region provide strong support for the hypothesis that flapping is a vortex-induced vibration. This indicates that flapping will not occur for small scale structures, which naturally exhibit small Reynolds numbers. This is borne out in the computational simulations of Ref. [11] at low Reynolds number ($\text{Re} < 50$). Interestingly, this is precisely the regime where cylinders do not exhibit periodic vortex-shedding, a prerequisite for vortex-induced vibrations.

## Acknowledgements

This research was supported by a grant of the Gordon and Betty Moore Foundation, the Human Resources Program in Energy Technology of the Korea Institute of Energy Technology Evaluation and Planning (KETEP), granted financial resource from the Ministry of Trade, Industry & Energy, Republic of Korea (No. 20134030200300), Caltech's Kavli Nanoscience Institute and the Australian Research Council grants scheme.

## References

[1] Anderson, J. D., *Fundamentals of Aerodynamics*, McGraw-Hill, Inc., New York, 1991.

[2] Argentina, M. and Mahadevan, L., Fluid-flow-induced flutter of a flag, *Proc. Nat. Acad. Sci.*, **102**, 2005, 1829–1834.

[3] Connell, B. S. H. and Yue, D. K. P., Flapping dynamics of a flag in a uniform stream, *J. Fluid Mech.*, **581**, 2007, 33–67.

[4] Gabbai, R. D. and Benaroya, H., An overview of modeling and experiments of vortex-induced vibration of circular cylinders, *J. Sound Vib.*, **282**, 2005, 575–616.

[5] Gilmanov, A., Le, T. B. and Sotiropoulos, F., A numerical approach for simulating fluid structure interaction of flexible thin shells undergoing arbitrarily large deformations in complex domains, *J. Comp. Phys.*, **300**, 2015, 814–843.

[6] Kim, D., Cossé, J., Huertas Cerdeira, C. and Gharib, M., Flapping dynamics of an inverted flag, *J. Fluid Mech.*, **736**, 2013, R1.

[7] Knisely, C. W., Strouhal numbers of rectangular cylinders at incidence: a review and new data, *J. Fluid Struct.*, **4**, 1990, 371–393.

[8] Kornecki, A., Dowell, E. H. and O'Brien, J., On the aeroelastic instability of two-dimensional panels in uniform incompressible flow, *J. Sound Vib.*, **47**, 1976, 163–178.

[9] Paidoussis, M. P., Price, S. J. and De Langre, E., *Fluid-Structure Interactions: Cross-Flow Instabilities*, Cambridge University Press, 2010.

[10] Rinaldi, S. and Paidoussis, M. P., Theory and experiments on the dynamics of a free-clamped cylinder in confined axial air-flow, *J. Fluid Struct.*, **28**, 2012, 167–179.

[11] Ryu, J., Park, S. G., Kim, B. and Sung, H. J., Flapping dynamics of an inverted flag in a uniform flow, *J. Fluid Struct.*, **57**, 2015, 159–169.

[12] Sader, J. E., Cossé, J., Kim, D., Fan, B. and Gharib, M., Large-amplitude flapping of an inverted-flag in a uniform steady flow – a vortex-induced vibration, *J. Fluid Mech.*, **793**, 2016, 524–555.

[13] Schmitz, F. W., *Aerodynamics of the model airplane. Part 1. Airfoil measurements*, Redstone Scientific Information Center, 1941.

[14] Shelley, M. J. and Zhang, J., Flapping and bending bodies interacting with fluid flows, *Annu. Rev. Fluid Mech.*, **43**, 2011, 449–465.

[15] Tang, C., Liu, N.-S. and Lu, X.-Y., Dynamics of an inverted flexible plate in a uniform flow, *Phys. Fluids*, **27**, 2015, 073601.

[16] Williamson, C. H. K. and Govardhan, R., Vortex-induced vibrations, *Annu. Rev. Fluid Mech.*, **36**, 2004, 413–455.